Coastal eutrophication drives acidification, oxygen loss, and ecosystem change in a major oceanic upwelling system

Faycal Kessouri[a,b,1], James C. McWilliams[b,1], Daniele Bianchi[b], Martha Sutula[a], Lionel Renault[b,c], Curtis Deutsch[d], Richard A. Feely[e], Karen McLaughlin[a], Minna Ho[a], Evan M. Howard[d], Nina Bednaršek[a,f], Pierre Damien[b], Jeroen Molemaker[b], and Stephen B. Weisberg[a]

[a]Department of Biogeochemistry, Southern California Coastal Water Research Project, Costa Mesa, CA 92626; [b]Department of Atmospheric and Oceanic Sciences, University of California Los Angeles, Los Angeles, CA 90095; [c]Laboratoire d'Études en Géophysique et Océanographie Spatiale, Institut de Recherche et de Developpement, CNRS, Université Paul Sabatier, Toulouse 31400, France; [d]School of Oceanography, University of Washington, Seattle, WA 98195; [e]Pacific Marine Environmental Laboratory, National Oceanic and Atmospheric Administration, Seattle, WA 98115; and [f]National Institute of Biology, Marine Biological Station Piran, 6330 Piran, Slovenia

Contributed by James C. McWilliams, March 2, 2021 (sent for review September 17, 2020; reviewed by Scott Doney and Marjorie A. M. Friedrichs)

Global change is leading to warming, acidification, and oxygen loss in the ocean. In the Southern California Bight, an eastern boundary upwelling system, these stressors are exacerbated by the localized discharge of anthropogenically enhanced nutrients from a coastal population of 23 million people. Here, we use simulations with a high-resolution, physical–biogeochemical model to quantify the link between terrestrial and atmospheric nutrients, organic matter, and carbon inputs and biogeochemical change in the coastal waters of the Southern California Bight. The model is forced by large-scale climatic drivers and a reconstruction of local inputs via rivers, wastewater outfalls, and atmospheric deposition; it captures the fine scales of ocean circulation along the shelf; and it is validated against a large collection of physical and biogeochemical observations. Local land-based and atmospheric inputs, enhanced by anthropogenic sources, drive a 79% increase in phytoplankton biomass, a 23% increase in primary production, and a nearly 44% increase in subsurface respiration rates along the coast in summer, reshaping the biogeochemistry of the Southern California Bight. Seasonal reductions in subsurface oxygen, pH, and aragonite saturation state, by up to 50 mmol m^{-3}, 0.09, and 0.47, respectively, rival or exceed the global open-ocean oxygen loss and acidification since the preindustrial period. The biological effects of these changes on local fisheries, proliferation of harmful algal blooms, water clarity, and submerged aquatic vegetation have yet to be fully explored.

coastal eutrophication | human impacts | acidification and oxygen loss | marine habitats | Southern California upwelling ecosystem

Human emissions of carbon dioxide (CO_2) to the atmosphere are driving global trends of warming, acidification, and oxygen (O_2) loss in the ocean (1), with deleterious consequences for marine ecosystems (2). In coastal regions, these global impacts overlap with the effects of anthropogenic nutrient inputs, particularly in shallow and enclosed bodies of water (3–5). Coastal eutrophication is most prominent in regions with large agricultural footprints and densely populated urban areas, where it has been linked to changes in ecosystem structure (6, 7) and declines in pH and O_2 concentrations (8, 9) that exacerbate the global trends (5, 10, 11).

In the California Current, a productive coastal region that supports important fisheries (12), wind-driven upwelling drives high biological productivity during spring and summer, exposing shelf waters to low-pH and low-O_2 conditions (13, 14). This natural variability makes the California Current exceptionally vulnerable to acidification and O_2 loss from global change (11, 15, 16). Strong upwelling and vigorous surface currents might suggest a minor role for coastal eutrophication in exacerbating these stressors (17); however, here, we find that the effect of local anthropogenically enhanced nutrient loads cannot be dismissed in this upwelling system.

Human activities are particularly intense in the Southern California Bight (SCB), an open embayment located between the Baja California Peninsula and Point Conception in the Southern California Current. This region hosts a variety of marine communities and hotspots of biodiversity (e.g., ref. 18), many of which benefit from environmental protection as Marine Protected Areas [MPAs (19)]. It is also home to a population of more than 23 million people, distributed along the coastline from Tijuana to Santa Barbara (20). Point and nonpoint source discharges to the ocean from this population are partitioned across 19 urban outfalls that discharge effluent from 23 wastewater treatment plants and 75 rivers, which release, on average, 8 million m^3 d^{-1} of nutrient-enriched water to the ocean. These nutrient sources rival natural upwelling in magnitude in the coastal waters of the SCB (21), roughly doubling available

Significance

We conduct a modeling study of the effects of enhanced coastal nutrient export from human activities on the carbon, nitrogen, and oxygen cycles of the Southern California Bight, in the context of emerging global climate change. The modeling approach used is innovative in the breadth of its scope, and simulations are generally consistent with local measurements. The human effects on the regional ecosystem from coastal nitrogen inputs of 23 million people are substantial, leading to significant increases in the photosynthesis and biomass of phytoplankton and increased oxygen loss and acidification of the water column. These changes are likely to compress habitat for a variety of marine organisms, with cascading ecological effects and implications for marine resources and water-quality management.

Author contributions: F.K., J.C.M., D.B., M.S., C.D., R.A.F., and S.B.W. designed research; F.K., J.C.M., D.B., M.S., L.R., C.D., R.A.F., M.H., E.M.H., N.B., and P.D. performed research; F.K., D.B., M.S., L.R., C.D., K.M., E.M.H., N.B., P.D., and J.M. contributed new reagents/analytic tools; F.K., J.C.M., D.B., M.S., L.R., K.M., M.H., and N.B. analyzed data; and F.K., J.C.M., D.B., M.S., and R.A.F. wrote the paper.

Reviewers: S.D., University of Virginia; and M.A.M.F., Virginia Institute of Marine Science, William & Mary.

The authors declare no competing interest.

[1]To whom correspondence may be addressed. Email: jcm@atmos.ucla.edu or faycalk@sccwrp.org.

This article contains supporting information online at https://www.pnas.org/lookup/suppl/doi:10.1073/pnas.2018856118/-/DCSupplemental.

Published May 17, 2021.

nitrogen within a coastal band of a few tens of kilometers, and making the SCB vulnerable to coastal eutrophication.

The SCB also hosts long-running monitoring programs that make it one of the best observed coastal ecosystems in the world. Among them, the California Cooperative Oceanic Fisheries Investigations (CalCOFI) program (22) samples the Bight quarterly each year, collecting hydrographic and biogeochemical measurements in coordination with the Southern California Coastal Ocean Observing System. These observations are augmented nearshore by quarterly surveys of water column and benthic parameters conducted collaboratively since 1990 by publicly owned treatment works (POTW) agencies as a part of their regulatory monitoring requirements (21, 23, 24). Yet, despite these intense monitoring efforts, and demonstrated improvements in benthic habitat conditions since adoption of the Clean Water Act, the influence of anthropogenic nutrient inputs on the pelagic habitats of the SCB remains poorly quantified, because observations cannot be used to disentangle the relative effects of local pollution, climate change, and natural variability.

In this study, we narrow this gap by conducting an assessment of the fate and consequences of anthropogenic nutrients discharged in the SCB, showing a range of cascading effects that could threaten marine ecosystems and biodiversity in the region. We conduct a series of simulations with a regional high-resolution, physical-biogeochemical model (*Materials and Methods*). The model is forced by realistic atmospheric fields and oceanic boundary conditions and by a new reconstruction of natural, non-point-source, and point-source river and ocean outfall discharges (25). We use a submesoscale-resolving configuration of the model, run at a horizontal resolution of 0.3 km over the SCB. This configuration is part of a suite of progressively finer-resolution simulations that translate global climate and circulation patterns to the coastal scales over which the release, dispersal, and biological utilization of anthropogenically enhanced nutrients occur. We show results from two hindcast simulations run for the period from January 1997 to December 2000.

The first simulation (CTRL) represents the regional biogeochemical dynamics in the absence of terrestrial nutrient inputs; the second (ANTH) includes inputs of dissolved inorganic and organic nitrogen and phosphorus, silicate, iron, and inorganic and organic carbon from rivers, wastewater outfalls, and atmospheric deposition (*Materials and Methods*). While these inputs contain both natural and anthropogenic sources, we estimate that 97% of total coastal nitrogen inputs are derived from point sources of treated wastewater effluent, while 2% are derived from nonpoint sources (urban and agricultural runoff) in the region (25). Thus, ANTH largely simulates the effects of nutrient and carbon enrichment of the SCB caused by human activities. The model is validated against in situ physical and biogeochemical observations from the Bight monitoring program, CalCOFI, and other data sources, including satellite observations (26). This validation shows an excellent agreement of the ANTH simulation with observations of nutrients, O_2, carbon, phytoplankton, and their dynamics. The period from January 1997 to December 2000 is chosen in order to capture the effects of the 1997–1998 El Niño.

Observed and Simulated Coastal Eutrophication

Eutrophication manifests as an increase of primary production above natural levels (27). While the bulk of the SCB is characterized by mesotrophic conditions (net primary production

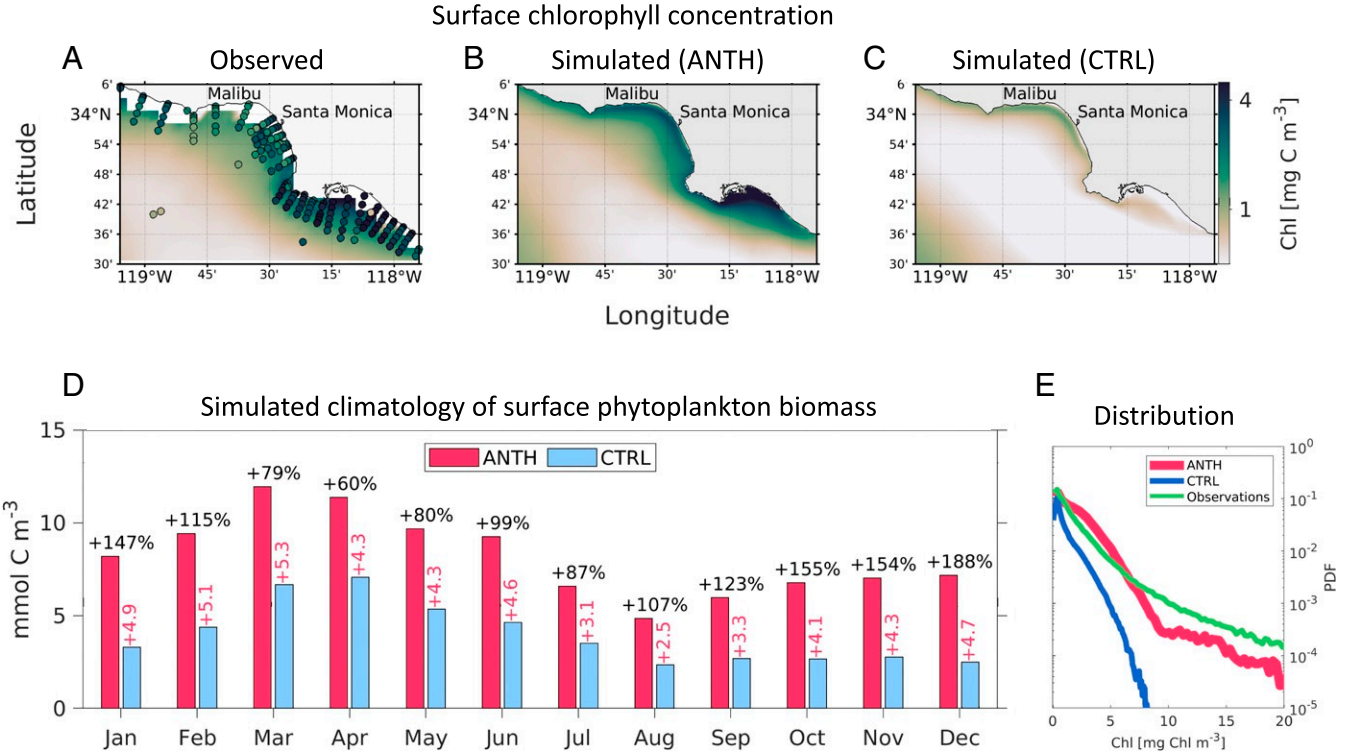

Fig. 1. Effects on coastal eutrophication in the SCB. (*A–C*) Four-year averages (January 1997 to December 2000) of surface chlorophyll concentration (mg Chl m^{-3}) from remote sensing and in situ data (*A*; filled circles are CalCOFI and POTW agency observations, and color contours satellite data) and from the ANTH and CTRL simulations respectively (*B* and *C*). (*D*) Simulated monthly climatology of surface phytoplankton biomass concentration (mmol C m^{-3}) in the 0- to 15-km coastal band of the Los Angeles and Orange County regions. The anthropogenic simulation (ANTH) is shown in red, and the control simulation with no terrestrial inputs (CTRL) in blue. Percent values on top of the bars show the change caused by anthropogenically enhanced inputs; pink numbers show the absolute difference between the two simulations. (*E*) Simulated (ANTH in red and CTRL in blue) and observed (green) probability distribution function of daily surface chlorophyll in the same area as *A–C* at 10-m depth.

>100 g C m^{-2} y^{-1}) (27) away from the coast, a band of high chlorophyll can be observed along the shelf, extending from the coast to about 15 km offshore (Fig. 1 *A*–*C*), as observed in ref. 28. Comparison of the CTRL and ANTH simulations shows that upwelling and mixing alone cannot maintain this high-chlorophyll band without the inclusion of anthropogenically enhanced terrestrial and atmospheric inputs represented in the ANTH simulation. Our simulations indicate that the persistent coastal high phytoplankton biomass in the SCB differs from the classic upwelling paradigm that dominates large swathes of the California Current further north (26). In the SCB, upwelling typically takes place between March and the beginning of summer, with a peak in April (Fig. 1*D*), when, in the absence of land-based and atmospheric inputs (CTRL), it would support average phytoplankton concentrations as high as 7 mmol C m^{-3} (1.1 mg Chl m^{-3}) 0 to 15 km from the shore. During the rest of the year, average phytoplankton concentrations would rarely exceed this threshold. In contrast, anthropogenically enhanced nutrient inputs (ANTH) drive coastal high phytoplankton biomass that consistently exceed 6 mmol C m^{-3} (1.1 mg Chl m^{-3}) year-round, with mean peak values observed in March on the order of 13 mmol C m^{-3} (2.2 mg Chl m^{-3}) (Fig. 1*D*).

On average, anthropogenically-enhanced nutrient inputs cause a nearly 2-fold increase in coastal (0–15 km) phytoplankton biomass concentrations (*SI Appendix*, Table S2), as compared to coastal upwelling alone. These nutrient sources further alter the spatial distribution of phytoplankton along the coast, dramatically increasing the occurrence of localized, high phytoplankton biomass (Fig. 1 *B* and *E*). While the largest concentrations driven by natural upwelling are observed north of Ventura and along the Santa Barbara coast in the CTRL simulation (26), terrestrial nutrients inputs drive persistent, or "chronic," high phytoplankton biomass (24) along the Los Angeles and Orange County coastlines (Fig. 1 *B* and *C*). Here, high-chlorophyll episodes exceeding 8 mg Chl m^{-3} are seen in the ANTH simulation, in agreement with observations (Fig. 1*E*). This increase in the frequency and intensity of high-biomass episodes is encapsulated by the frequency distribution of chlorophyll in the SCB (Fig. 1*E*), which reveals a doubling of the number of events exceeding 2.2 mg Chl m^{-3} and a nearly 20-fold increase for events exceeding 5 mg Chl m^{-3}.

Nutrient Sources Driving Coastal Eutrophication

Comparison of the ANTH and CTRL simulations shows that nitrogen enrichment drives the persistent coastal high phytoplankton biomass in the SCB (Fig. 2). Nitrogen is the primary limiting nutrient in the SCB (29), supplied to coastal waters by oceanic and terrestrial pathways. The oceanic circulation transports nitrate into the euphotic zone via upwelling and mixing. Terrestrial sources introduce a combination of nitrate, ammonium, and organic nitrogen via three major routes: atmospheric deposition, rivers, and submarine wastewater outfalls. The combined input from these three pathways, including Mexican transboundary flows to the Tijuana River watershed into US coastal waters, during January 1997 to December 2000 was 188,000 kg N d^{-1} (*SI Appendix*, Table S1). This represents an estimated 75-fold increase relative to the natural terrestrial sources that would have occurred during the preindustrial period (25). Dissolved inorganic nitrogen loads during the present day have declined ∼7% from the historic simulation period, due to nitrogen management that has occurred at several POTWs to support potable water recycling (25). These changes can be contextualized by considering a longer time series of POTW inputs and regulation of ocean discharges. These coastal outfalls have no nitrogen limits in discharge permits, while inland river nitrate and ammonium criteria have generally kept dissolved inorganic nitrogen concentrations below 70 mmol m^{-3} (25). Organic nitrogen loads from large POTWs (effluent discharge > 2.19 m^3 s^{-1}) have declined 73% since the early 1970s, due to improved organic solids management and reduction in biological oxygen demand. In contrast, total dissolved inorganic nitrogen loads from these outfalls have increased 35% from the 1970s to the current day, because of a regional population increases of 66%, although individual outfalls have documented declines since their peaks in the 1990s (*SI Appendix*, Fig. S3). Natural, point, and nonsource inputs directly to Mexican coastal waters are not included in this simulation. The relative contribution of land-based and atmospheric nutrient sources is shown in *SI Appendix*, Table S1. Atmospheric deposition and riverine runoff are minor pathways for coastal nitrogen inputs relative to ocean outfalls, representing around 5% and 10%, respectively, of the total coastal nitrogen inputs. POTW outfalls released approximately 142,000 kg N d^{-1} of inorganic nitrogen to coastal waters in the SCB between January 1997 and December 2000, mainly as dissolved ammonium, the concentration of which exceeds nitrate by tenfold to hundredfold in treated wastewater.

Submarine outfalls were designed to release wastewater as nutrient-enriched plumes below the pycnocline (30). Because they are fresher than ambient seawater, these plumes rise to

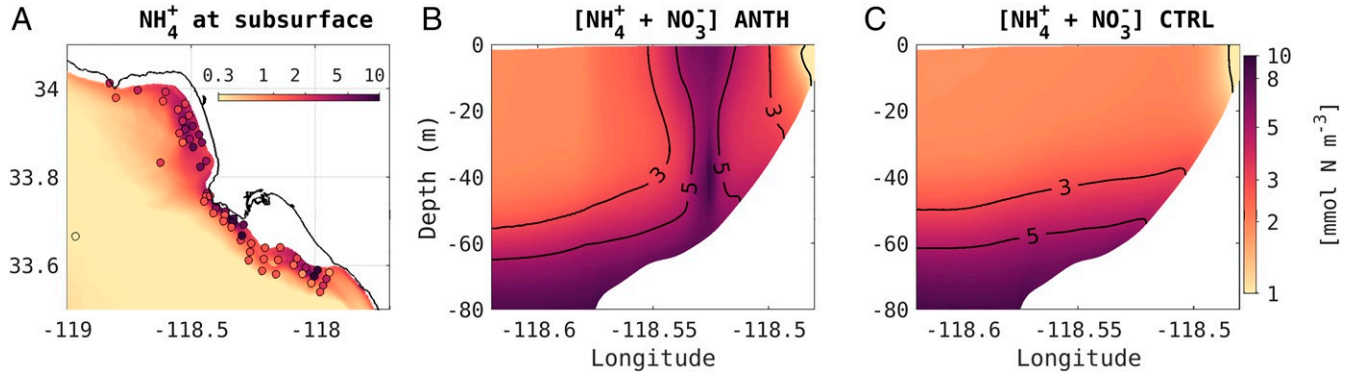

Fig. 2. (*A*) Subsurface (30 to 45 m) ammonium (NH_4^+) concentration (mmol m^{-3}) averaged during summer (June to August between 1997 and 2000) from the ANTH simulation (background color contours) and in situ observations (colored dots), showing the location and dispersal of ammonium-enriched wastewater plumes near the coast. Blue stars show the location of three large POTW outfalls. A detailed illustration of the coast-wide inputs is presented in *SI Appendix*, Fig. S1. Oceanic regions shallower than 30 m in the Santa Monica and San Pedro shelves are shown in white in *A*. (*B* and *C*) Dissolved inorganic nitrogen (nitrate plus ammonium, NO_3^- + NH_4^+, in mmol m^{-3}) averaged during winter along a cross-shore section in the Santa Monica Bay, shown by the solid black line in *A*, where *B* is the ANTH simulation and *C* is the CTRL simulation. Weak wintertime stratification allows shoaling of buoyant plumes and mixing, exposing anthropogenically enriched waters to the surface, evident in *B*.

neutrally buoyant depths of about 30 to 45 m (26, 31) and then are swept along isobaths by the alongshore-flowing coastal current (Fig. 2*A*). The model simulations show that this release strategy is mostly effective in preventing nutrients from reaching the surface during the stratified summer season. However, wintertime cooling, intense winds, and submesoscale circulation events periodically deepen the surface mixed layer to encompass wastewater, exposing excess nutrients to the euphotic zone (Fig. 2).

Under natural conditions, ammonium concentrations would rarely exceed 1 mmol N m^{-3} in the euphotic layer, a small concentration compared to nitrate (*SI Appendix*, Fig. S4). However, both observations and the ANTH simulation commonly show ammonium concentrations greater than 5 mmol N m^{-3}, with values up to 15 mmol N m^{-3}, near San Pedro and in the Santa Monica Bay, two regions heavily affected by POTW outfalls (Fig. 2 *A* and *B*; *SI Appendix*, Fig. S4). These high ammonium concentrations cannot be reconciled with the natural nitrogen cycle in the region and are evidence of the entrainment of buoyant wastewater nitrogen in surface waters (Fig. 2*B*; *SI Appendix*, Fig. S4). Nitrogen-enriched waters are further swept into the variable nearshore northward current that flows past the Orange County and Los Angeles coastlines and dispersed over a wider region toward the central and northern SCB. In the southern SCB, the Point Loma POTW outfall near San Diego releases wastewater deep enough that it generally remains below the reach of wintertime mixing; however, we caveat that these simulations do not include wastewater inputs directly to watersheds of Playas Rosario and Ensenada in northern Baja California.

Biogeochemical Consequences of Eutrophication

Amplification of Coastal Productivity. Coastwide, phytoplankton productivity integrated over the euphotic zone (0 to 40 m) increases from an average of 88 mmol C m^{-2} d^{-1} 0 to 15 km from the shore in the CTRL simulation to 109 mmol C m^{-2} d^{-1} in the ANTH simulation—a 23% enhancement. The largest differences between the simulations are observed in the San Pedro and Santa Monica Bays, where productivity increases by 80% and 42%, respectively, due to large local inputs (*SI Appendix*, Table S3). Beyond these hotspots, productivity increases broadly along the coast (Fig. 3 *A* and *B*), driven by the interplay between local sources and horizontal transport, from 50% along Los Angeles and Orange County, to 22% in Orange County, and about 24% in Southern San Diego. Productivity and phytoplankton biomass increase significantly during winter and early spring, when mixing exposes nutrient-enriched waters to the surface. The interaction between subsurface nutrient buildup, vertical mixing, and surface productivity is further illustrated by the response to oceanic variability during the October 1997 to March 1998 El Niño (*SI Appendix*, Fig. S6). At the peak of this event, the deepening of the pycnocline and anomalously strong stratification reduced the input of nitrate to surface waters by natural upwelling (*SI Appendix*, Fig. S7). Although rapidly nitrified (32) (*SI Appendix*, Fig. S8), anthropogenically derived ammonium became the main source of inorganic nitrogen to surface waters, driving the largest amplification of primary production and maintaining levels similar to regular coastal upwelling events, despite the widespread decrease in productivity offshore.

Increase of Organic Matter Export. Because of uptake of ammonium from anthropogenic sources, the ANTH simulation shows a 23% increase in new production coastwide in the upper layer (0 to 40 m), where 30 to 40% of the total primary production is supported by external nitrogen inputs, one-third of which is from land-based sources (*SI Appendix*, Table S3). This increase in new production is balanced by a similar increase in organic matter export, which is enhanced coastwide by about 24% (Fig. 3*D*; *SI Appendix*, Table S4). This is achieved in the model by a shift in phytoplankton assemblages, which become dominated by large phytoplankton and diatoms. This ecological reorganization facilitates production of large aggregates that intensify the flux of sinking organic matter (Fig. 3*D*; *SI Appendix*, Table S4). In parallel, subduction and lateral transport of nonsinking organic matter are also enhanced in the ANTH simulation.

Enhanced O_2 Loss and Acidification. Following eutrophication, inorganic carbon uptake and O_2 production increase significantly in the surface waters of the SCB (*SI Appendix*, Table S3), driving increased rates of remineralization at depth. In summer, the average respiration rate between 40 and 80 m increases

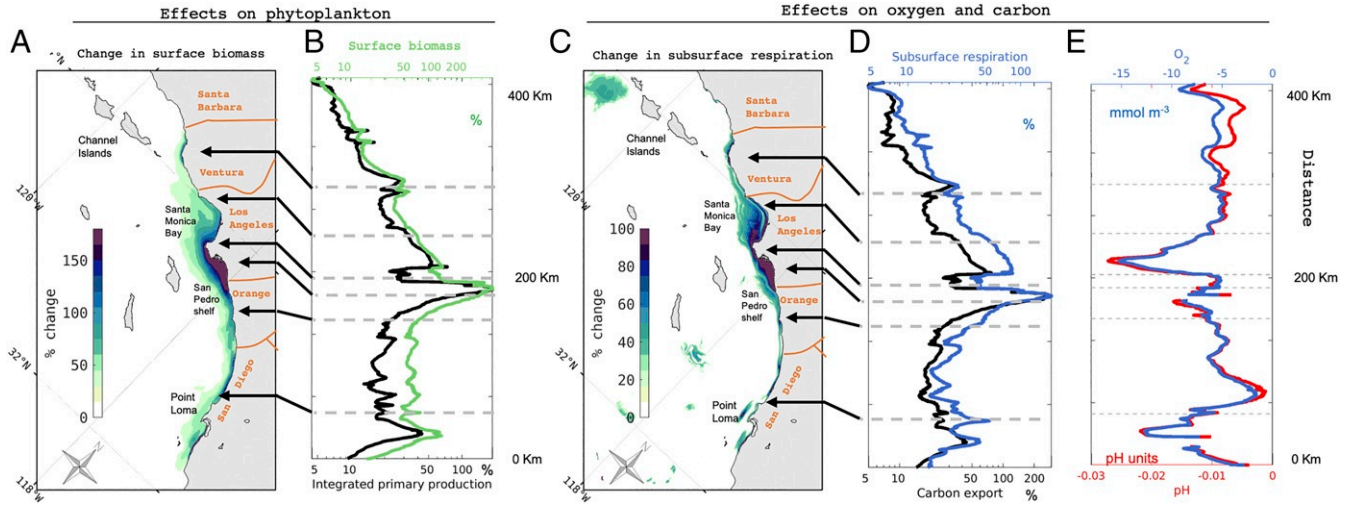

Fig. 3. Biogeochemical effects of land-based and atmospheric nutrient inputs in the SCB. (*A*) Surface chlorophyll enhancement (%) in the ANTH simulation, relative to the CTRL simulation. (*B*) Alongshore surface chlorophyll (green line) and vertically integrated net primary production (0 to 80 m, black line) enhancement (%). (*C*) Subsurface (40 to 80 m) respiration enhancement (%). (*D*) Alongshore subsurface (40 to 80 m) respiration and carbon export enhancement (%). (*E*) Absolute alongshore O_2 (mmol m^{-3}; blue line) and pH (seawater scale; red line) changes at 50-m depth. Values show spring and summer averages between January 1997 and December 2000. Alongshore values are the averages between the coast and 15 km offshore. Note the nonlinear *x* axis in *B* and *D*. Names of counties and their boundaries are labeled in orange in *A* and *C*.

coastwide by 44% (Fig. 3 *C* and *D*; *SI Appendix*, Table S5), from about 6.4 mmol O_2 m^{-2} d^{-1} in the CTRL to 9.3 mmol O_2 m^{-2} d^{-1} in the ANTH simulation—a value comparable to other coastal regions affected by rapid O_2 loss (17).

Spatial variations in respiration rates mirror those in the phytoplankton biomass and productivity response to eutrophication (*SI Appendix*, Table S5). During the stratified late spring and summer periods, O_2 concentrations increase slightly at the surface and decrease at depth (40 m) by up to 50 mmol m^{-3} (55 mmol m^{-3} during El Niño) coastwide, with larger reductions in regions most affected by outfall discharge (Los Angeles and Santa Monica) (Fig. 4*A*; *SI Appendix*, Table S6). This O_2 deficit is removed during well-mixed fall and winter periods (Fig. 4*B*).

Similarly, nutrient uptake drives an increase in surface pH and in the saturation state of aragonite (Ω_{Ar}), a form of calcium carbonate mineral used by a variety of shell-building organisms, while decreasing those variables at depth (Fig. 4 *B*–*D*). Subsurface acidification (Fig. 4*F*) follows seasonal and interannual patterns similar to O_2 loss (Fig. 4*C*) and is also generally removed by a combination of winter mixing (*SI Appendix*, Fig. S11) and gas exchange, which tends to equilibrate O_2, and, at a slower rate, CO_2 with the atmosphere.

Nutrient-driven O_2 loss and acidification were strongest during the 1997–1998 El Niño because of the greater stratification during the spring and summer months (*SI Appendix*, Fig. S5). For example, Ω_{Ar} decreased by up to 0.63 (38%) during El Niño versus 0.47 (28%) in the following period. Despite this impact, stratification during El Niño kept Ω_{Ar} above 1.45 (200 mmol O m^{-3}) at 40 m depth.

Changes in Coastal Emissions of Greenhouse Gases. The greater uptake of inorganic carbon by photosynthesis drives an anomalous CO_2 flux from the atmosphere to the ocean in the ANTH simulation, which is superimposed by those caused by global changes in atmospheric CO_2 and sea-surface temperature. Thus, following eutrophication, coastal waters sequester an additional 1.55×10^{12} g C y^{-1} in the 0 to 15 km from the shore of the SCB over the period between January 1997 and December 2000 (*SI Appendix*, Table S7). However, this uptake is compensated by an increase in emissions of N_2O, a greenhouse gas approximately 300 times more powerful than CO_2 (33). Increased remineralization and direct inputs of ammonium, in particular from deep outfalls, intensify nitrification at depth (*SI Appendix*, Fig. S8), enhancing the formation of N_2O, a byproduct of ammonium oxidation. Throughout the summer, additional N_2O accumulates in subsurface layers, emerging at the surface during winter. Surface N_2O saturation reaches up to 135% in the ANTH simulation (*SI Appendix*, Fig. S9), driving the additional emission of 3.76×10^{10} g N_2O y^{-1} (*SI Appendix*, Table S10) to the atmosphere (7.53×10^9 g N_2O y^{-1} in the Los Angeles region alone).

Implications for the Coastal Ecosystem

Effects on Fisheries and Vulnerable Habitats. Local shifts in O_2 and carbon caused by terrestrial inputs coincides with global O_2 loss and acidification trends that threaten a variety of marine resources (34). In the California Current, these include shell-forming organisms that are sensitive to reductions in pH and Ω_{Ar}, e.g., calcifying zooplankton such as pteropods (35), benthic echinoderms, crustaceans (36), mollusks (37), and detritus feeders (38), plus a variety of fish and invertebrates that live at the limit of their erobic habitat (39). Relatively small reductions in O_2, in combination with global warming and deoxygenation, could drive habitat compression, population declines and exclusion from the region (39), while reductions in pH and Ω_{Ar} could

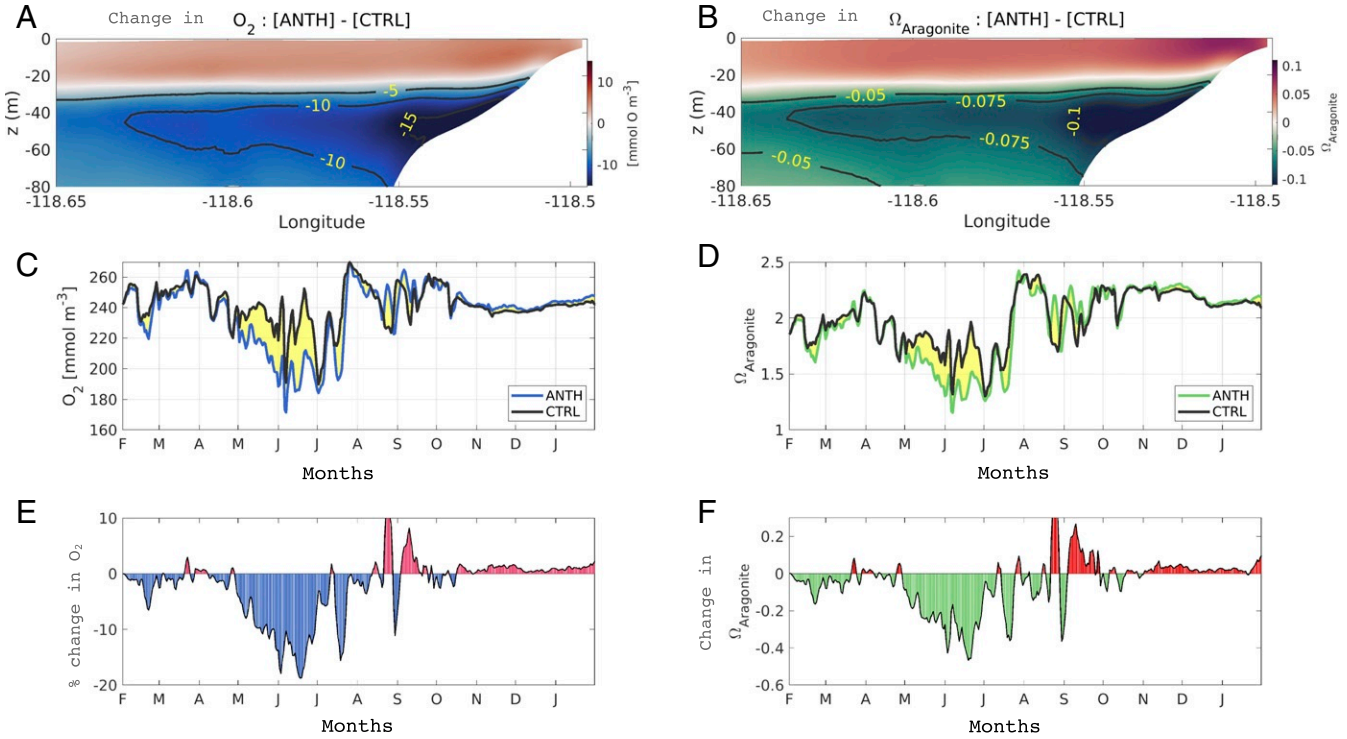

Fig. 4. (*A* and *B*) Changes in O_2 (*A*) and Ω_{Ar} (*B*) caused by anthropogenically enhanced nutrient inputs (ANTH minus CTRL simulations) in the Santa Monica Bay, along the cross-shore section marked with a black line in Fig. 2*A* averaged during spring–summer between years 1997 and 2000. (*C* and *D*) Time series of one full year from February 1997 to February 1998 of O_2 (*C*) and Ω_{Ar} (*D*) at 50-m depth averaged over the Los Angeles coast. The solid black line shows the CTRL simulation and the colored lines the ANTH simulation. The difference between ANTH and CTRL is highlighted in yellow. (*E* and *F*) Average relative O_2 change (100 × [ANTH − CTRL]/CTRL) (*E*) and average absolute Ω_{Ar} change (ANTH − CTRL) (*F*) at 50-m depth in the Los Angeles coast. Eutrophication increases O_2 and Ω_{Ar} at the surface, due to enhanced photosynthesis, and decreases them below the surface, due to enhanced respiration.

negatively impact ecosystem dynamics (35, 36). From a temporal perspective, species that reside in the SCB experience the greatest acidification from spring to summer, coinciding with the most prolific reproductive and growing season, potentially inducing the largest impact on vulnerable early-life stages. Because of temporal and vertical habitat compression, the impact is likely to be most severe in the 30- to 80-m layer of the water column for pelagic calcifiers, such as pteropods, larval decapods, and bivalves (Fig. 4*A*).

Anthropogenically enhanced nutrient inputs cause nearshore reductions in Ω_{Ar} and pH of 0.11 and 0.012, on average, and as high as 0.63 and 0.10, respectively (Fig. 4 and *SI Appendix*, Tables S8 and S9). These changes would drive pH and Ω_{Ar} below the thresholds for pteropod mild and severe dissolution, reduced calcification, and compromised growth (40). They would also impair growth of larval and juvenile oysters and mussel larvae, for which Ω_{Ar} thresholds of 1.4, 1.8, and 2.0, respectively, have been observed (41–44), and potentially induce crab exoskeleton dissolution (36). Despite the localized nature of nutrient-induced acidification, increased retention around POTW discharges, in particular during the more quiescent summer period, could prolong exposure to unfavorable acidified conditions. Combined acidification and O_2 loss can further exacerbate habitat compression. While warming and O_2 reduction may be sufficient to drive significant erobic habitat loss (39), they should be examined in combination with reductions in pH, in light of synergistic impacts on early life stages [e.g., fish larvae, (45)]. Lastly, enhanced photosynthesis in the upper 30 m reduces the severity of ocean acidification, potentially alleviating some negative impacts on surface-dwelling species, not only directly via increased pH and Ω_{Ar} (Fig. 4), but also indirectly via increased phytoplankton biomass, which could confer a degree of resilience to acidification by increasing prey availability and offsetting the metabolic demands from acclimation to acidification (46). The strongest effects of eutrophication overlap with several marine refuges in the SCB, including national parks, national marine sanctuaries, and state MPAs (*SI Appendix*, Fig. S1). Some of the largest effects occur in state reserves such as Point Dume, north of the Santa Monica Bay (MPA2 in *SI Appendix*, Fig. S1), and at Point Vicente and Abalone Cove (MPA3 in *SI Appendix*, Fig. S1), located off the Palos Verdes peninsula (*SI Appendix*, Tables S3, S6, S8, and S9). At the latter site, the average surface chlorophyll increases by nearly fivefold above natural values; primary production and subsurface respiration double; and subsurface O_2 and pH decrease by up to 54 mmol m^{-3} and 0.1 respectively. Additional work is needed to investigate the consequences of these combined changes for the marine ecosystem.

Effects on Water Clarity and Submerged Aquatic Vegetation. The SCB hosts giant kelp and seagrass beds that improve water quality, reduce coastal erosion, and provide refuges that foster biodiversity and fisheries. While anthropogenically enhanced nitrogen inputs along the coast could augment growth, increased phytoplankton biomass reduces water clarity and light availability, potentially compressing viable habitats for these macroflora (47, 48). We illustrate the effect of increasing water turbidity on submerged aquatic vegetation by considering changes in light penetration driven by eutrophication. Giant kelp growth occurs at irradiance levels typically exceeding 1.8 W m^{-2} (49). In the ANTH simulation, this light threshold shoals by about 8 m along the Los Angeles coast. More broadly throughout the SCB, the euphotic depth (where irradiance is reduced to 1% the surface value) shoals by 5 m on average and up to 17 m in regions more strongly affected by eutrophication (*SI Appendix*, Fig. S10). The interplay between nutrient increase and light reduction remains a key uncertainty in evaluating the net effect of coastal eutrophication on submerged aquatic vegetation in the SCB (47).

Linkages to Harmful Algal Blooms. The ANTH simulation shows a shift in biomass toward diatoms. This finding supports an emerging hypothesis that anthropogenically enhanced nutrient inputs may exacerbate the magnitude and frequency of harmful algal blooms in the SCB. In this region, blooms of the toxigenic diatom genus *Pseudo-nitzschia* are associated with upwelling of cold, nutrient-rich waters, occurring from late winter to summer (50). A marked difference exists between northern and southern waters in the SCB, with maximum concentrations of the *Pseudo-nitzschia* neurotoxin domoic acid in shellfish tissue observed from late spring to fall north of Los Angeles, and from winter to spring south of it (50). A series of *Pseudo-nitzschia* blooms observed in coastal waters near Palos Verdes, Newport Beach, and San Diego (51, 52) were not associated with upwelling events, and no evidence of relationship between nutrients and rainfall was found. The timing and location of these blooms are consistent with the results from the ANTH simulation, where eutrophication hotspots are largely driven by subsurface anthropogenic nitrogen sources, and tend to initiate earlier than wind-driven upwelling. Further research is needed to establish a mechanistic linkage between anthropogenic nutrient and carbon inputs and the prevalence of harmful *Pseudo-nitzschia* blooms in the region.

Conclusions and Implications for Management

Our findings indicate that anthropogenically enhanced nitrogen inputs drive eutrophication in the SCB, exacerbating global acidification and O_2 loss, despite vigorous ocean circulation in the region. The POTW outfalls that contribute the majority of these inputs are designed to prevent the emergence of nutrient-laden waters into the euphotic zone; however, our simulations indicate that vigorous mixing and submesoscale currents (53) periodically expose wastewater plumes to the surface, fertilizing coastal waters, and enhancing the production of organic matter and its decomposition at depth (Fig. 3).

The magnitude of this contribution varies spatially and temporally, depending on upwelling, stratification, and circulation. During spring and summer, subsurface O_2 loss and acidification from local anthropogenic inputs can be comparable to, or greater than, those expected from global climate change. For example, land-based and atmospheric nutrient inputs reduce dissolved O_2, pH, and Ω_{Ar} by up to 50 mmol m^{-3}, 0.09, and 0.47 respectively, compared to global average reductions of approximately 5 mmol m^{-3}, 0.1, and 0.5 driven by climate change and the oceanic uptake of anthropogenic carbon (54, 55), which are generally enhanced in coastal waters (11, 56, 57). For comparison, Earth system models project a decline of 18 mmol O_2 m^{-3} in the CCS between 2000 and 2100 (39). As noted elsewhere (10, 58), the decline in seawater buffering capacity caused by anthropogenic CO_2 uptake exacerbates the pH and Ω_{Ar} reduction caused by eutrophication, an effect that may be further amplified by local atmospheric CO_2 emissions from the city of Los Angeles (59).

That nutrient emissions from dense urban agglomerations can drive significant biogeochemical changes has implications for management strategies, particularly given the high cost of nutrient nonpoint source control and wastewater-treatment-plant upgrades. Additional science is needed to inform those strategies, premier among which is translating the chemical changes (Fig. 3) into biological responses. A growing body of research indicates that calcifying plankton, shellfish, and crustaceans are affected by the decline in the saturation state of calcium carbonate (35) and that the combined effects of reduced carbonate ion, decreasing dissolved O_2 and rising temperatures are causing habitat compression for fish (39). However, biologically relevant acidification and dissolved O_2 water-quality criteria, with which to assess the magnitude of those impacts, have not been yet developed (60).

There is also a need for additional model simulations that place our findings into a broader context. For instance, the simulations need to be extended to present-day nutrient loading and climate to reflect changes over the last two decades. Attribution is needed to quantify relative effects of point, nonpoint, and natural sources on productivity, oxygen loss, and acidification, as the present simulations only differentiate the combined effects of land-based and atmospheric nutrients. The effects of realistic management options need to be quantified. In particular, policy conversations should be further informed by simulations targeting the efficacy of nutrient management versus other resource recovery options, such as wastewater recycling or nutrient removal by kelp aquaculture, and how the outcomes of local actions compare to those from investments in global CO_2 reduction.

Materials and Methods

We use the Regional Ocean Modeling System, ROMS (61), coupled to the Biogeochemical Elemental Cycling model, BEC (62). The model domain covers the SCB, from Tijuana to Pismo Beach (*SI Appendix*, Figs. S1 and S2). The model configuration has a horizontal resolution of 300 m and a vertical resolution of 60 σ-coordinate levels and represents the last of a series of dynamical downscaling simulations (12, 4, 1, and 0.3 km, respectively, *SI Appendix*, Fig. S2), in which progressively higher-resolution domains are forced by boundary conditions from the next coarser-resolution domain. Lateral boundary conditions come from the 1-km simulation (53), and surface boundary conditions from an atmospheric simulation with the Weather Research and Forecast model run at 6-km resolution (63). More information on the model setup is provided in refs. 29 and 63. We run two simulations, the first representing only the natural oceanic cycles of nutrients (CTRL), and the second adding nutrient (NO_3^-, NO_2^-, NH_4^+, $Si(OH)_4$, PO_4^{3-}, and Fe), inorganic carbon, alkalinity, and dissolved organic matter (N, C, and P) inputs from terrestrial anthropogenic sources (ANTH) (64). Both simulations include the effects of anthropogenic global warming and atmospheric CO_2 increase as part of the boundary conditions. Terrestrial sources consist of POTW outfalls, rivers, and atmospheric deposition. Wastewater effluent data are based on permit monitoring databases, and river discharges on model simulations and monitoring data that capture both surface-water storm flow and baseflow conditions (25). Outfalls and rivers are implemented as point sources, following ref. 31. Atmospheric deposition is derived from the Community Multiscale Air Quality model and implemented following ref. 5. The model is validated against a comprehensive database of physical and biogeochemical observations (65) from the SCB and provides a realistic representation of physical and biogeochemical cycles in the SCB (26). The model code is available at 10.5281/zenodo.3988618 (66), the in situ data used for model validation at 10.5281/zenodo.3988574 (67), and local land-based and atmospheric nutrient input data at 10.5281/zenodo.4448224 (64). The statistical analyses are applied on the 0–10 km coastal band along the following subregions: Santa Barbara, Ventura, Santa Monica, San Pedro shelf, Orange County, North and South San Diego. The Greater Los Angeles region covers the 0–15 km coastal band from Point Dume to Laguna Beach and includes the Santa Monica and San Pedro Bays. The distribution of the subregions is illustrated in *SI Appendix*, Fig. S1

Data Availability. The model code, in situ data used for model validation, and local land-based and atmospheric nutrient input data are available at Zenodo (10.5281/zenodo.3988618, 10.5281/zenodo.3988574, and 10.5281/zenodo.4448224, respectively).

ACKNOWLEDGMENTS. This research was supported by National Oceanic and Atmospheric Administration (NOAA) Grants NA15NOS4780186 and NA15NOS4780191; California Ocean Protection Council Grant C0100400; and NSF Grant OCE-1419450. This work was supported by the NOAA under Ecosystem and Harmful Algal Bloom (ECOHAB) Award NA18NOS4780174. This is ECOHAB publication 980. Computational resources were provided by the Extreme Science and Engineering Discovery Environment through allocation TG-OCE170017; and by the supercomputer Hoffman2 at the University of California Los Angeles, at the Institute for Digital Research and Education. This is contribution No. 5157 from the NOAA Pacific Marine Environmental Laboratory. We thank Kristen Foley and Robin Dennis (USEPA National Exposure Research Laboratory) for providing the output from the Community Multiscale Air Quality Model, corrected over ocean surface with Tropical Rainfall Measuring Mission data.

1. T. F. Stocker *et al.*, "Climate change 2013: The physical science basis" in *Contribution of Working Group I to the Fifth Assessment Report of the Intergovernmental Panel on Climate Change*, T. F. Stocker et al., eds. (Cambridge University Press, Cambridge, UK, 2013).
2. H.-O. Pörtner *et al.* "Ocean systems" in *Climate Change 2014: Impacts, Adaptation, and Vulnerability. Part A: Global and Sectoral Aspects. Contribution of Working Group II to the Fifth Assessment Report of the Intergovernmental Panel on Climate Change*, C. B. Field *et al.*, Eds. (Cambridge University Press, Cambridge, UK, 2014), pp. 411–484.
3. R. E. Turner, N. N. Rabalais, Coastal eutrophication near the Mississippi River delta. *Nature* **368**, 619–621 (1994).
4. W. M. Kemp *et al.*, Eutrophication of Chesapeake Bay: Historical trends and ecological interactions. *Mar. Ecol. Prog. Ser.* **303**, 1–29 (2005).
5. S. C. Doney *et al.*, Impact of anthropogenic atmospheric nitrogen and sulfur deposition on ocean acidification and the inorganic carbon system. *Proc. Natl. Acad. Sci. U.S.A.* **104**, 14580–14585 (2007).
6. R. Elmgren. Man's impact on the ecosystem of the Baltic Sea: Energy flows today and at the turn of the century. *Ambio*, 326–332 (1989).
7. V. H. Smith, S. B. Joye, R. W. Howarth, Eutrophication of freshwater and marine ecosystems. *Limnol. Oceanogr.* **51**, 351–355 (2006).
8. R. B. Wallace, H. Baumann, J. S. Grear, R. C. Aller, C. J. Gobler, Coastal ocean acidification: The other eutrophication problem. *Estuar. Coast Shelf Sci.* **148**, 1–13 (2014).
9. N. N. Rabalais *et al.*, Eutrophication-driven deoxygenation in the coastal ocean. *Oceanography* **27**, 172–183 (2014).
10. W.-J. Cai *et al.*, Acidification of subsurface coastal waters enhanced by eutrophication. *Nat. Geosci.* **4**, 766 (2011).
11. D. Breitburg *et al.*, Declining oxygen in the global ocean and coastal waters. *Science* **359**, eaam7240 (2018).
12. F. P. Chavez, M. Messié, A comparison of eastern boundary upwelling ecosystems. *Prog. Oceanogr.* **83**, 80–96 (2009).
13. R. A. Feely, C. L. Sabine, J. M. Hernandez-Ayon, D. Ianson, B. Hales, Evidence for upwelling of corrosive" acidified" water onto the continental shelf. *Science* **320**, 1490–1492 (2008).
14. F. Chan *et al.*, Emergence of anoxia in the California Current large marine ecosystem. *Science* **319**, 920 (2008).
15. N. Gruber *et al.*, Rapid progression of ocean acidification in the California Current system. *science* **337**, 220–223 (2012).
16. N. S. Lovenduski, R. X. Brady, S. G. Yeager, M. C. Long, Skillful multiyear predictions of ocean acidification in the California Current System. *Nat. Commun.* **11**, 2166 (2019).
17. K. Fennel, J. M. Testa, Biogeochemical controls on coastal hypoxia. *Annu. Rev. Mari. Sci.* **11**, 105–130 (2019).
18. R. S. Steneck *et al.*, Kelp forest ecosystems: Biodiversity, stability, resilience and future. *Environ. Conserv.* **29**, 436–459 (2002).
19. A. Rassweiler, C. Costello, D. A. Siegel, Marine protected areas and the value of spatially optimized fishery management. *Proc. Natl. Acad. Sci. U.S.A.* **109**, 11884–11889 (2012).
20. US Census Bureau. County population totals (2008) https://www.census.gov/data/datasets/time-series/demo/popest/2010s-counties-total.html (Accessed 7 January 2020).
21. M. D. A. Howard *et al.*, Anthropogenic nutrient sources rival natural sources on small scales in the coastal waters of the Southern California Bight. *Limnol. Oceanogr.* **59**, 285–297 (2014).
22. S. McClatchie, *Regional Fisheries Oceanography of the California Current System* (Springer, Dordrecht, Netherlands, 2016).
23. K. McLaughlin *et al.*, Seasonal patterns in aragonite saturation state on the southern California continental shelf. *Continent. Shelf Res.* **167**, 77–86 (2018).
24. N. P. Nezlin *et al.*, Spatial and temporal patterns of chlorophyll concentration in the Southern California Bight. *J. Geophys. Res.: Oceans* **123**, 231–245 (2018).
25. M. Sutula *et al.*, Dataset of terrestrial fluxes of freshwater, nutrients, carbon, and iron to the Southern California Bight, U.S.A.*Data Brief* **35**, 106802 (2021).
26. F. Kessouri *et al.*, Configuration and validation of an oceanic physical and biogeochemical model to investigate coastal eutrophication in the Southern California Bight. Earth Space Sci. Open Archive [Preprint] (2021) https://www.essoar.org/doi/10.1002/essoar.10504012.1 (Accessed 23 December 2020).
27. S. W. Nixon, Coastal marine eutrophication: A definition, social causes, and future concerns. *Ophelia* **41**, 199–219 (1995).
28. A. J. Lucas *et al.*, The green ribbon: Multiscale physical control of phytoplankton productivity and community structure over a narrow continental shelf. *Limnol. Oceanogr.* **56**, 611–626 (2011).
29. C. A. Deutsch *et al.*, Biogeochemical variability in the California current system. bioRxiv [Preprint] (2021) https://www.biorxiv.org/content/10.1101/2020.02.10.942565v1 (Accessed 23 December 2020).
30. R. C. Y. Koh, N. H. Brooks, Fluid mechanics of waste-water disposal in the ocean. *Annu. Rev. Fluid Mech.* **7**, 187–211 (1975).
31. Y. Uchiyama, E. Y. Idica, J. C. McWilliams, K. D. Stolzenbach, Wastewater effluent dispersal in southern California bays. *Continent. Shelf Res.* **76**, 36–52 (2014).
32. K. McLaughlin *et al.*, Rapid nitrification of wastewater ammonium near coastal ocean outfalls, Southern California, USA.*Estuarine Coast. Shelf Sci.* **186**, 263–275 (2017).
33. P. Ciais *et al.*, "Carbon and other biogeochemical cycles" in *Climate Change 2013: The Physical Science Basis. Contribution of Working Group I to the Fifth Assessment Report of the Intergovernmental Panel on Climate Change*, T. F. Stocker *et al.*, Eds. (Cambridge University Press, Cambridge, UK, 2014), pp. 465–570.

34. S. C. Doney *et al.*, Climate change impacts on marine ecosystems. *Annu. Rev. Mari. Sci.* **4**, 11–37 (2012).
35. N. Bednarsek *et al.*, Systematic review and meta-analysis towards synthesis of thresholds of ocean acidification impacts on calcifying pteropods and interactions with warming. *Front. Mari. Sci.* **6**, 227 (2019).
36. N. Bednaršek *et al.*, Exoskeleton dissolution with mechanoreceptor damage in larval dungeness crab related to severity of present-day ocean acidification vertical gradients. *Sci. Total Environ.* **716**, 136610 (2020).
37. E. A. Aalto *et al.*, Abalone populations are most sensitive to environmental stress effects on adult individuals. *Mar. Ecol. Prog. Ser.* **643**, 75–85 (2020).
38. E. E. Hodgson *et al.*, Consequences of spatially variable ocean acidification in the California Current: Lower pH drives strongest declines in benthic species in southern regions while greatest economic impacts occur in northern regions. *Ecol. Model.* **383**, 106–117 (2018).
39. E. M. Howard *et al.*, Climate-driven aerobic habitat loss in the California current system. *Sci. Adv.* **6**, eaay3188 (2020).
40. A. R. Gunderson, E. J. Armstrong, J. H. Stillman, Multiple stressors in a changing world: The need for an improved perspective on physiological responses to the dynamic marine environment. *Annu. Rev. Mari. Sci.* **8**, 357–378 (2016).
41. A. Barton, B. Hales, G. G. Waldbusser, C. Langdon, R. A. Feely, The Pacific oyster, *Crassostrea gigas*, shows negative correlation to naturally elevated carbon dioxide levels: Implications for near-term ocean acidification effects. *Limnol. Oceanogr.* **57**, 698–710 (2012).
42. B. Hales, I. Gimenez, G. G. Waldbusser, Ocean acidification stress index for shellfish (oasis): Linking pacific oyster larval survival and exposure to variable carbonate chemistry regimes. *Elem. Sci. Anth.* **6**, 51 (2018).
43. A. Hettinger *et al.*, Persistent carry-over effects of planktonic exposure to ocean acidification in the Olympia oyster. *Ecology* **93**, 2758–2768 (2012).
44. B. Gaylord *et al.*, Functional impacts of ocean acidification in an ecologically critical foundation species. *J. Exp. Biol.* **214**, 2586–2594 (2011).
45. E. DePasquale, H. Baumann, C. J. Gobler, Vulnerability of early life stage northwest Atlantic forage fish to ocean acidification and low oxygen. *Mar. Ecol. Prog. Ser.* **523**, 145–156 (2015).
46. L. Ramajo *et al.*, Food supply confers calcifiers resistance to ocean acidification. *Sci. Rep.* **6**, 19374 (2016).
47. M. S. Foster, D. R. Schiel, Loss of predators and the collapse of southern California kelp forests (?): Alternatives, explanations and generalizations. *J. Exp. Mar. Biol. Ecol.* **393**, 59–70 (2010).
48. L. W. Tait, Giant kelp forests at critical light thresholds show compromised ecological resilience to environmental and biological drivers.*Estuarine Coast. Shelf Sci.* **219**, 231–241 (2019).
49. T. A. Dean, F. R. Jacobsen, Growth of juvenile *Macrocystis pyrifera* (Laminariales) in relation to environmental factors. *Mar. Biol.* **83**, 301–311 (1984).
50. J. Smith *et al.*, Co-occurring dissolved algal toxins observed at multiple coastal sites in southern California via solid phase adsorption toxin tracking. *Toxicon* **171**, 62–65 (2019).
51. A. Schnetzer *et al.*, Blooms of *Pseudo-nitzschia* and domoic acid in the San Pedro channel and Los Angeles harbor areas of the Southern California Bight, 2003–2004. *Harmful Algae* **6**, 372–387 (2007).
52. L. B. Busse *et al.*, Domoic acid in phytoplankton and fish in San Diego, CA, USA. *Harmful Algae* **5**, 91–101 (2006).
53. F. Kessouri *et al.*, Submesoscale currents modulate the seasonal cycle of nutrients and productivity in the California Current system. *Global Biogeochem. Cycles* **34**, e2020GB006578 (2020).
54. J. C. Orr *et al.*, Anthropogenic ocean acidification over the twenty-first century and its impact on calcifying organisms. *Nature* **437**, 681–686 (2005).
55. S. Schmidtko, L. Stramma, M. Visbeck, Decline in global oceanic oxygen content during the past five decades. *Nature* **542**, 335–339 (2017).
56. S. C. Doney, The growing human footprint on coastal and open-ocean biogeochemistry. *Science* **328**, 1512–1516 (2010).
57. J. A. T. Booth *et al.*, Patterns and potential drivers of declining oxygen content along the southern California coast. *Limnol. Oceanogr.* **59**, 1127–1138 (2014).
58. R. A. Feely *et al.*, The combined effects of acidification and hypoxia on pH and aragonite saturation in the coastal waters of the California Current ecosystem and the northern Gulf of Mexico. *Continent. Shelf Res.* **152**, 50–60 (2018).
59. S. Feng *et al.*, Los Angeles megacity: A high-resolution land–atmosphere modelling system for urban CO_2 emissions. *Atmos. Chem. Phys.* **16**, 9019–9045 (2016).
60. S. B. Weisberg *et al.*, Water quality criteria for an acidifying ocean: Challenges and opportunities for improvement. *Ocean Coast Manag.* **126**, 31–41 (2016).
61. A. F. Shchepetkin, An adaptive, courant-number-dependent implicit scheme for vertical advection in oceanic modeling. *Ocean Model.* **91**, 38–69 (2015).
62. J. K. Moore, S. C. Doney, K. Lindsay, Upper ocean ecosystem dynamics and iron cycling in a global three-dimensional model. *Global Biogeochem. Cycles* **18**, GB4028 (2004).
63. L. Renault *et al.*, The physical structure and behavior of the California current system. bioRxiv [Preprint] (2021) https://www.biorxiv.org/content/10.1101/2020.02.10.942730v1 (Accessed 23 December 2020).
64. M. Sutula *et al.*, A baseline of terrestrial freshwater and nitrogen fluxes to the Southern California Bight, USA. Zenodo. https://doi.org/10.5281/zenodo.4448224. Accessed 12 August 2020.
65. F. Kessouri *et al.*, Collection of in situ monitoring data in the Southern California Bight 1950-2017 for model validation. Zenodo. https://doi.org/10.5281/zenodo.4536641. Deposited 17 August 2020.
66. F. Kessouri *et al.*, ROMS-BEC oceanic physical and biogeochemical model code for the Southern California Current System V2020. Zenodo. https://doi.org/10.5281/zenodo.3988618. Deposited 17 August 2020.
67. F. Kessouri *et al.*, Collection of in situ monitoring data in the Southern California Bight 1950-2017 for model validation. Zenodo. https://doi.org/10.5281/zenodo.3988574. Deposited 17 August 2020.